http://dx.doi.org/10.5516/NET.02.2013.009

SECOND ATLAS DOMESTIC STANDARD PROBLEM (DSP-02) FOR A CODE ASSESSMENT

YEON-SIK KIM*, KI-YONG CHOI, SEOK CHO, HYUN-SIK PARK, KYOUNG-HO KANG, CHUL-HWA SONG, and WON-PIL BAEK
Thermal Hydraulics Safety Research Division, Korea Atomic Energy Research Institute
1045 Daedeokdaero, Yuseong-gu, Daejeon 305-353, Rep. of Korea
*Corresponding author. E-mail : yskim3@kaeri.re.kr

Received February 04, 2013
Accepted for Publication June 07, 2013

KAERI (Korea Atomic Energy Research Institute) has been operating an integral effect test facility, the Advanced Thermal-Hydraulic Test Loop for Accident Simulation (ATLAS), for transient and accident simulations of advanced pressurized water reactors (PWRs). Using ATLAS, a high-quality integral effect test database has been established for major design basis accidents of the APR1400 plant. A Domestic Standard Problem (DSP) exercise using the ATLAS database was promoted to transfer the database to domestic nuclear industries and contribute to improving a safety analysis methodology for PWRs. This 2nd ATLAS DSP (DSP-02) exercise aims at an effective utilization of an integral effect database obtained from ATLAS, the establishment of a cooperation framework among the domestic nuclear industry, a better understanding of the thermal hydraulic phenomena, and an investigation into the possible limitation of the existing best-estimate safety analysis codes. A small break loss of coolant accident with a 6-inch break at the cold leg was determined as a target scenario by considering its technical importance and by incorporating interests from participants. This DSP exercise was performed in an open calculation environment where the integral effect test data was open to participants prior to the code calculations. This paper includes major information of the DSP-02 exercise as well as comparison results between the calculations and the experimental data.

KEYWORDS : ATLAS, Integral Effect Test, DVI, SBLOCA, Thermal-Hydraulic, DSP

1. INTRODUCTION

1.1 Background and Brief History

The first Domestic Standard Problem (DSP-01) exercise using ATLAS was completed successfully by holding a final workshop in April, 2010. Though the DSP-01 was the first cooperative program for code validation based on an integral effect database, most major domestic organizations, including industries, universities and research institutes, volunteered to contribute to strengthening the technical infrastructure for code validation and to expanding a domestic cooperative network. Technical information sharing and discussion was active between experienced code users. In particular, the water levels of the reactor core and downcomer regions, ECC bypass rate, multi-dimensional phenomena in the downcomer region, loop seal clearing phenomena, and loop flow characteristics were identified as the crucial phenomena for a close investigation from the viewpoint of code modeling. There were un-experienced code users among the participants and they benefited greatly from this valuable course of exercise. In conclusion, the DSP-01 was a major landmark in the validation of the thermal-hydraulic safety analysis codes. More details can be found in the final comparison report [1] and related paper [2].

A second Domestic Standard Problem (DSP-02) exercise was launched in July, 2010. In the kick-off meeting, the outcome of the DSP-01 was analyzed and discussed by the participants. Noticeable major outcomes were that the DSP-01 provided an opportunity for major domestic nuclear organizations to pursue MARS-KS code validation against qualified IET data and to provide a cooperation network. The know-how and expertise of experienced code users were spread among participants. On the contrary, however, user effects were remarkable owing to great differences in code experience among the code users, and this caused the user effects overshadow the possible code deficiencies. In particular, qualification of the code initialization was highlighted to ensure correct transient calculations. Another lesson from the DSP-01 was that we need to focus on detailed thermal-hydraulic phenomena rather than see only the overall aspects that contribute to a practical code validation. Thus, it was suggested and agreed upon that each participant was responsible for providing an additional analysis on at least one special topic in the DSP-02.

Among the several test scenarios carried out by KAERI, a 6-inch cold leg break SBLOCA test was proposed and accepted as a target test item of the DSP-02. Most participants

agreed that the 6-inch cold leg break SBLOCA would be interesting in view of a practical safety analysis. In addition, special assessment topics relevant to code validation were proposed such as 1) 2D behavior in the downcomer, 2) break flow modeling, 3) 3D behavior in the reactor pressure vessel, 4) loop seal clearing, 5) ECC bypass, 6) heat loss modeling, 7) reactor pressure vessel bypass, and so on. In the kick-off meeting, a draft specification of the DSP-02 [3] was distributed along with an updated facility description report (FDR) [4].

1.2 Objectives of the ATLAS DSP-02

A best-estimate safety analysis methodology for small break LOCAs including the DVI line break accidents needs to be developed to identify the uncertainties involved in the safety analysis results. Such a best-estimate safety analysis methodology will contribute to defining a more precise specification of the safety margin and thus will lead to a greater operational flexibility. However, such an effort was lacking because the available integral effect test data were not sufficient.

The current DSP-02 aims at the following:

- Effective utilization of an integral effect database obtained from ATLAS.
- Expanding cooperation network among the domestic nuclear industry, academic institutes, research institute, and regulation organizations.
- Safety analysis technology transfer to inexperienced code users.
- Better understanding of thermal hydraulic phenomena in the upper annulus downcomer region during the DVI injection period of SBLOCAs.
- Investigation of the possible limitation of the existing best-estimate safety analysis codes.

1.3 Host Organization

The ATLAS DSP-02 program, like the DSP-01, was organized in collaboration with KINS. KAERI was responsible for a general coordination of the DSP-02, data provisioning, information on the ATLAS facility and DSP-02, code calculation, receipt of submissions, result comparisons, progress meetings, final workshop, and comparison report. As a joint operation agency, KINS was responsible for coordination support, code calculation, progress meetings, and the final workshop.

1.4 List of Participants

In the second ATLAS DSP program (DSP-02), thirteen organizations eventually signed an agreement as listed in Table 1. Each signatory organization had an obligation to perform an open calculation within the exercise period using the test results provided by the operating agency, KAERI. Most participants used the best-estimate system code, MARS-KS, and a few participants used the RELAP5 code, and all the participants were also requested to write their analysis results including special assessment topics in an assigned section of the final comparison report [5]. Unfortunately, an organization did not manage to finish its calculation owing to a shortage of manpower, as shown in Table 1.

1.5 Special Code Assessment Topics

In the previous DSP-01 program, significantly great user effects were found among the participants. In fact, such great user effects were caused by differences in facility modeling and differences in experiences between skillful and inexperienced code users. Such user effects made it difficult to find the code deficiencies independently. Thus, significant effort has been placed on minimizing the user effects and on assessing the code prediction capability itself based on experimental data.

In the DSP-02, it was agreed that each participant was responsible for performing a sensitivity analysis on at least one special code assessment topic. This activity is expected to help find the code deficiencies and obtain user guidelines that can minimize the "user effects." As the MARS-KS code was utilized by most participants, this special code assessment activity provided an intensive code assessment environment. Eight code assessment items were defined at the beginning of this program by a discussion among the participants: (1) break flow modeling, (2) loop seal clearing behavior, (3) ECC bypass, (4) RPV bypass, (5) heat loss effects, (6) momentum effects of DVI nozzle, (7) 2-D behavior in the downcomer region, (8) and others, and assigned them to each participant, as shown in the remarks of Table 1.

Table 1. List of DSP-02 Participants

	Participants (Organization)	Code	Remark
1	KEPRI	MARS-KS	ECC Bypass
2	KINS	MARS-KS	Loop Seal Clearing
3	NETEC	RELAP5/MOD3.3	Break Flow Model
4	Doosan Heavy Industry	MARS-KS	Break Flow Model
5	KEPCO NF	RELAP5/MOD3.3	RPV and ECC Bypasses
6	KEPCO E&C	RELAP5-ME	ECC Momentum Effect
7	SNU	MARS-KS	2-D Behavior in DC
8	EN2T	MARS-KS	Loop Seal Clearing
9	FNC	MARS-KS	Loop Seal Clearing
10	RETECH	MARS-KS	Break Flow Model
11	SENTECH	MARS-KS	Heat Loss Effect
12	SDD	MARS-KS	Withdrawal
13	KAERI	MARS-KS	Operating Agency

2. THE ATLAS FACILITY AND TEST DESCRIPTION

2.1 Overview of ATLAS

ATLAS is a thermal-hydraulic integral effect test facility for evolutionary pressurized water reactors of APR1400 and OPR1000. The reference plant of ATLAS is the APR1400, which is an advanced power reactor developed by the Korean industry and has a rated thermal power of 4000 MW and a loop arrangement of 2 hot legs and 4 cold legs for the reactor coolant system [6,7]. ATLAS also incorporates some specific design features of the Korean standard nuclear power plant, the OPR1000, such as a cold-leg injection mode for a safety injection and a low pressure safety injection mode. ATLAS can be used to investigate the multiple responses between the systems for a whole plant or between the subcomponents in a specific system during anticipated transients and postulated accidents.

ATLAS has the same two-loop features as the APR1400 and is designed according to the well-known scaling method suggested by Ishii and Kataoka [8] to simulate various test scenarios as realistically as possible. It is a half-height, 1/288 -volume scaled test facility with respect to the APR1400. The main motive for adopting the reduced-height design is to allow for an integrated annular downcomer where the multidimensional phenomena can be important in some accident conditions with a DVI operation. According to the scaling law, the reduced height scaling has time-reducing results in the model. For a one-half-height facility, the time for the scaled model is $\sqrt{2}$ times faster than the prototypical time. The friction factors in the scaled model are maintained the same as those of the prototype. The hydraulic diameter of the scaled model is maintained the same as that of the prototype to preserve the prototypical conditions for the heat transfer coefficient. Major scaling parameters of ATLAS are summarized in Table 2.

The configuration of ATLAS for a cold leg SBLOCA consists of a primary system, a secondary system, a safety injection system, a break simulating system, a containment simulating system, and auxiliary systems as shown in Fig. 1. The primary system includes a reactor vessel, two hot legs,

Table 2. Major Scaling Parameters of ATLAS

Parameters	Scaling law	ATLAS design
Length	l_{0R}	1/2
Diameter	d_{0R}	1/12
Area	d_{0R}^2	1/144
Volume	$l_{0R}\, d_{0R}^2$	1/288
Core DT	ΔT_{0R}	1
Velocity	$l_{0R}^{1/2}$	$1/\sqrt{2}$
Time	$l_{0R}^{1/2}$	$1/\sqrt{2}$
Power/Volume	$l_{0R}^{-1/2}$	$\sqrt{2}$
Heat flux	$l_{0R}^{-1/2}$	$\sqrt{2}$
Core power	$l_{0R}^{1/2}\, d_{0R}^2$	1/203.6
Flow rate	$l_{0R}^{1/2}\, d_{0R}^2$	1/203.6
Pressure drop	l_{0R}	1/2

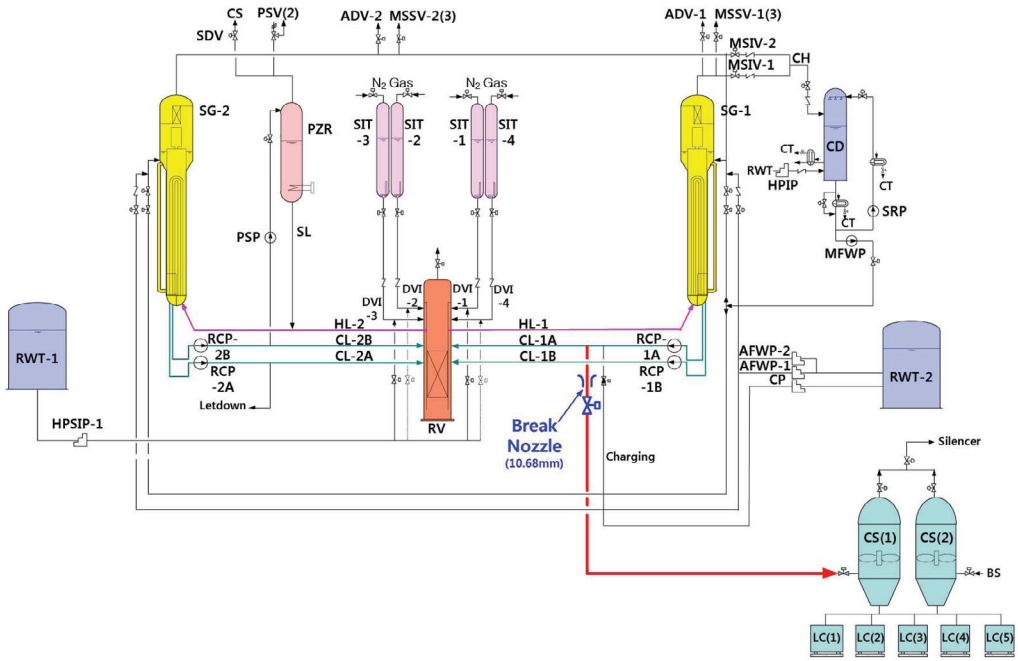

Fig. 1. Configuration of the ATLAS Facility for Cold Leg SBLOCA

four cold legs, a pressurizer, four reactor coolant pumps, and two steam generators. The secondary system of ATLAS is simplified to be of a circulating loop type. The steam generated at two steam generators is condensed in a direct condenser tank, and the condensed feedwater is again injected into the steam generators. Most of the safety injection features of the APR1400 and OPR1000 plants are incorporated into the safety injection system of ATLAS. It consists of four safety injection tanks (SITs), a high pressure safety injection pump (SIP) that can simulate a safety injection and long term cooling, a charging pump for charging an auxiliary spray, and a shut down cooling pump and a shutdown heat exchanger for low pressure safety injection, shutdown cooling operation, and recirculation operation. The break simulation system consists of several break simulating lines such as LBLOCA, a DVI line break LOCA, SBLOCA, SGTR, MSLB, and FLB. Each break simulating line consists of a quick opening valve, a break nozzle, and instruments. It is precisely manufactured to have a scaled break flow through it, as shown in Fig. 2. The containment simulating system of ATLAS has a function of collecting the break flow rate and maintaining a specified back-pressure to simulate a containment atmosphere. In addition, ATLAS has some auxiliary systems such as a makeup system, a component cooling system, a nitrogen/air/steam supply system, a vacuum system, and a heat tracing system. The detailed design and description of the ATLAS development program can be found in reference 9.

2.2 Experimental Condition and Procedure of the SB-CL-09 Test

In the present experimental test, SB-CL-09, a small break LOCA was assumed primarily to occur at a cold leg-1A piping located between the outlet of the RCP-1A and the corresponding RV inlet nozzle. In addition, a single-failure of a loss of a diesel generator, resulting in the minimum safety injection flow to the reactor pressure vessel, was assumed to occur in concurrence with the reactor trip. Therefore, the SI water from the SIP is only injected through the DVI-1 and -3 nozzles and the SI water from the SIT is injected through all of the DVI nozzles.

2.2.1 Actual Test Conditions

The present test conditions were determined by a pre-test calculation with a best-estimate thermal hydraulic code, MARS 3.1. First, a transient calculation was performed for the 6-inch SBLOCA of the APR1400 to obtain the reference initial and boundary conditions. A best-estimate safety analysis methodology, which is now commonly accepted in nuclear industries, was applied to the transient calculation of the APR1400. A single failure assumption for a safety injection system was assumed in the MARS calculation; four SITs and two of the SIPs were utilized during the test period. The initial and boundary conditions were obtained by applying the scaling ratios, shown in Table 2 to the MARS calculation results for the APR1400. Table 3 compares the rated steady-state condition between the APR1400 and ATLAS for the SBLOCA test.

There are four bypass valves connected to the downcomer in the ATLAS. Two bypass valves of FCV-RV-37 and FCV-RV-38 are between the downcomer and the upper head, and two bypass valves of FCV-RV-95 and FCV-RV-96 are between the downcomer and hot legs. The two bypass valves of FCV-RV-37 and FCV-RV-38 should be opened by 74% and 65%, respectively, to provide the required flow rate of 0.25 kg/s each, and the two bypass valves of FCV-RV-95 and FCV-RV-96 should be opened by 81% and 97%, respectively, to provide the required flow rate of 0.71 kg/s each.

2.2.2 Test Procedure

Prior to a transient test, several actions were taken. They included an instrument calibration with the ATLAS system drained, purging and filling the ATLAS system including leakage tests, an instrument calibration with the water-filled primary system, and an implementation of test specific control logics into the process control computers for sequence control. The sequence control logics

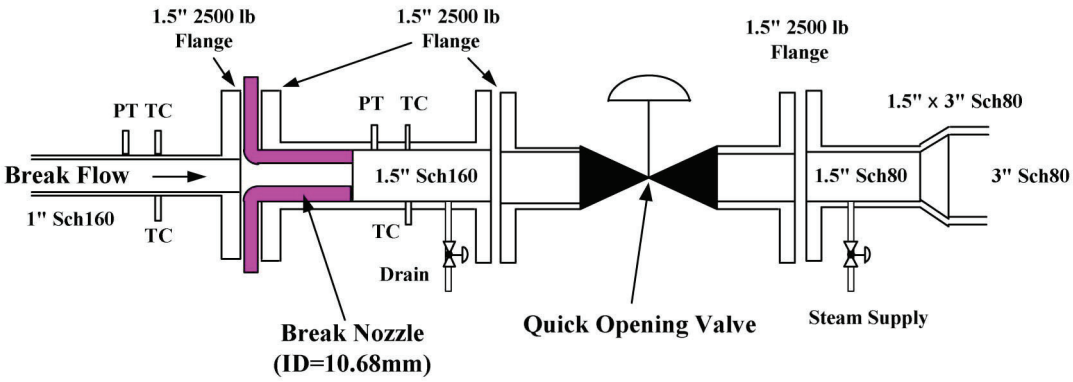

Fig. 2. Configuration of a Break Simulator for 6" Cold Leg SBLOCA

Table 3. Calculated Initial Conditions for the SB-CL-09

Design parameters	APR1400 (P) (Steady State)	ATLAS (M) (Steady State)	Ratio (P/M)
Reactor vessel			
Normal power, MWt	3983.00	1.56	2,553.21
Pressurizer pressure, MPa	15.50	15.50	1.00
Core exit temp, ºC	324.20	324.20	1.00
Core inlet temp, ºC	291.30	290.70	1.00
Temp. rise, ºC	32.90	33.50	0.98
Core flow, kg/s	20275.00	7.99	2,537.55
Steam generator			
Steam flow rate, kg/s (SG-1)	1152.40	0.44	2,619.09
Steam flow rate, kg/s (SG-2)	1152.40	0.44	2,619.09
Saturated steam pressure, MPa	6.90	7.83	0.88
Steam temp., ºC	284.90	293.50	0.97
Primary piping			
Hot leg flow, kg/s	10496.00	3.99	2,630.58
Cold leg flow, kg/s	5540.10	1.99	2,783.97
Hot leg temp., ºC	323.30	323.80	1.00
Cold leg temp., ºC	291.30	289.60	1.01
Heat transfer rate (W)	2044.80	0.77	2,655.58

executed the required control actions for the corresponding control devices such as the main core heater, RCP, SIP, and valves.

Reaching a specified initial condition of the whole system for the test, as shown in Table 4, the steady-state conditions of the primary and secondary system were maintained for more than 30 minutes. After this steady-state period, the main test started by an opening of the break simulation valve, OV-BS-06. With the start of the test, the primary system pressure decreased rapidly below 10.7 MPa, which was the set-point of the low-pressurizer pressure (LPP) signal. When the LPP signal occurred, the RCP and pressurizer heater stopped, and the main feed water isolation valves and the SIP were actuated with specified delay times. Further decreasing the primary pressure to below 4.03 MPa resulted in a passive injection of the SIT water. Tables 5 and 6 show the scheduled sequence of events and the actual progress of the events observed in the SB-CL-09.

2.2.3 Sequence of Events

After an opening of the break simulation valve, OV-BS-06, the test sequence was controlled by the corresponding control logic, which defined the set-point and related time delay, as shown in Table 5. When the pressurizer pressure measured by PT-PZR-01 decreased below 10.7 MPa, an LPP signal was issued. After the LPP signal, RCPs and pressurizer heater were tripped with no time delay, and the reactor was tripped with a 0.354 s delay. The closing of the main feed water isolation valves and the actuation of the SIPs was scheduled to occur with 7.08 s and 28.29 s delays from the LPP signal, respectively. The SIT injection was initiated by the low upper downcomer pressure (LUDP). The actual sequence of events during the SB-CL-09 was presented in Table 6.

2.2.4 Core Power and Heat Balance

The initial steady-state heat balance was checked by comparing the applied core power with the heat removal rate through two SGs calculated by steam flow rates and temperature differences between the feed water and the main steam. Fig. 3 shows a heat balance at a steady state condition of the SB-CL-09. The total applied power was about 1,633 kW and the total removal heat energy through the two SGs was up to about 1,471 kW. There is a 162 kW difference between the applied and removed power owing to the heat loss of the system, including the primary and secondary systems.

The heat loss from the primary system into the environment cannot be completely prevented even though thick insulation materials envelop the reactor pressure vessel and the primary pipelines. The heat loss was estimated by the following simplified empirical correlation [4];

$$Q_{loss,1} = 0.32 \cdot (T_w - T_{atm}), \quad (1)$$

where, T_W is the outer wall surface temperature measured at the middle of the reactor pressure vessel, and T_{atm} is atmospheric temperature measured on the test day.

The heat loss from each steam generator into the environment was also estimated according to the empirical correlation [4].

$$Q_{loss,2} = 0.00077 \cdot (T_w - T_{atm})^{1.8843}, \quad (2)$$

Table 4. Actual Initial and Boundary Conditions of the SB-CL-09

Parameter	Measured value	Instruments	Remarks [1)]
Primary system			
- Core power (MW)	1.633	-	Including heat loss
- Heat loss (kW)	66/57	Primary/Secondary	Estimated value
- PZR Pressure (MPa)	15.5	PT-PZR-01	Pressurizer Figure 4.1.15
- Core inlet temp. (K)	563.2	TF-LP-02G18	Inlet plenum Figure 4.1.2
- Core exit temp.(K)	598.8	TF-CO-07-G14,G18,G21, G25	Averaged Figure 4.1.6
- Hot leg temp. (K)	597.7 598.7	TF-HL1-03A TF-HL2-03A	Hot leg 1 Figure 4.1.8 Hot leg 2 ditto
- Cold leg temp. (K)	565.4 565.5 564.2 565.3	TF-CL1A-04A TF-CL1B-04A TF-CL2A-04A TF-CL2B-04A	Cold leg 1A Figure 4.1.10 Cold leg 1B ditto Cold leg 2A ditto Cold leg 2B ditto
- RCS flow rate (kg/s)	2.2 ± 5% 2.2 ± 5% 2.2 ± 5% 2.2 ± 5%	QV-CL1A-01B QV-CL1B-01B QV-CL2A-01B QV-CL2B-01B	Cold leg 1A Figure 4.1.17 Cold leg 1B ditto Cold leg 2A ditto Cold leg 2B ditto
- Core bypass flow rate (kg/s)	0.49 1.36	Downcomer to upper head Downcomer to hot leg	Estimated value
- Pressurizer level (m)	3.83	LT-PZR-01	Figure 4.1.21
Secondary system	(SG1/SG2)		
- Pressure (MPa)	7.82/7.82	PT-SGSD1-01/PT-SGSD2-01	Figure 4.1.16
- Steam temp. (K)	566.9/566.7 568.5/568.8	TF-MS1-01/TF-MS2-01 TF-SGSD1-03/TF-SGSD2-03	Main steam line Steam dome Figure 4.1.12
- FW temp. (K)	505.4/506.4 496.5/495.7	TF-MF1-01/TF-MF2-01 TF-MF1-02/TF-MF2-02	Economizer inlet Downcomer inlet
- FW flow rate (kg/s)	0.373/0.382 0.044/0.042	QV-MF1-01/QV-MF2-01 QV-MF1-02/QV-MF2-02	Economizer inlet Figure 4.1.18 Downcomer inlet ditto
- Water level (m)	1.95/2.0	LT-SGSDDC1-01/ LT-SGSDDC2-01	Figure 4.1.22
- Heat removal(MW)	0.673/0.752	-	Approximation
- Heat loss(kW)	28.5/28.5	-	Estimated value
ECCS			
- SIT pressure (MPa)	4.24/4.15/ 4.01/4.17	PT-SIT1,2,3,4-02	Figure 4.1.23
- SIT temp. (K)	322.5/323.2/ 323.2/325.4	TF-SIT1,2,3,4-03	Ditto
- SIT level (%)	95.1/94.9/ 94.2/94.5	LT-SIT1,2,3,4-01 (5.32/5.30/5.25/5.27)	Ditto (meter)
- RWT temp. (K)	321.2	TF-RWT-01	ECC water storage tank
Containment - Pressure (MPa)	0.1013	Atmospheric condition	Open

Note. 1) All the figures represented on these remarks can be referred to reference 4.

where, T_W is averaged values of the temperatures measured at the outer wall surface of the steam generators, and T_{atm} is the atmospheric temperature.

The estimated heat losses through the primary and secondary systems are about 87 kW and 62 kW, respectively. The estimated heat loss through the system can be seen in Fig. 4.

2.2.5 Identified Thermal Hydraulic Phases during the SB-CL-09

Compared with a large break LOCA, the phases of the small break LOCA prior to core recovery occurred over a long period. To identify various phenomena, a small break LOCA can be divided into five phases: a blowdown, natural circulation, loop seal clearance, boil-off, and core recovery [10]. The duration of each phase depends on the break size and performance of the ECCS. In the SB-CL-09, the five characteristic phases were clearly identified, and they were compared with the characteristic parameters such as the primary pressure (PT-PZR-01), secondary pressure (PT-SGSD1-01), and collapsed water level of the downcomer (LT-RPV-04A) in Fig. 5. Detailed

Table 5. Scheduled Sequence of Events of the SB-CL-09

Event Description (SOE Signal)	Action by Operator/Control Logic	Condition	Check Point or Description
Heat-up	Trend logging start	Heat-up stage	Trend logging status Follow the heat-up procedure
Preheating	BS/CS line Preheating	- Quasi-steady-state - RPV bypass value - SIT water level & temperature - RWT water level and temperature, 50℃ - Primary coolant flow rate: 8% of the scaled value	1) Trip logic and set point 2) Core power distribution 3) Tracing heater status
Data Acquisition	DAS start	Steady State - Initial Core Power: 1.566 MWe - Primary/secondary Press.: 15.5/7.8 MPa - Hot leg flow rate : 3.98 kg/s - Hot/Cold Temperature.: 323.9/289.3 ℃ - SG water level: 2.0 m (LT-SGSDDC1,2-01), 5.0 m (LT-SGSDRS1,2-01) - MSSV Auto-setting	1) Data storage space 2) DAS status
Steady-state Initial Status Checking	Primary /Secondary /Safety Injection /Break System /Containment Simulating System		Check for steady-state
Break Start	OV-BS-06 Opening		
LPP		PT-PZR-01 < 10.721 MPa	
RCP Trip	RCP Stop	LPP + 0.0 s delay	
PZR Heater Off		LPP + 0.0 s delay	
Reactor Scram	Table control	LPP + 0.354 s delay	
Main Feedwater Isolation	Isolation valve close	LPP + 7.08 s delay	MSSV-01 bank OPEN/CLOSE (8.1/7.7 MPa)
SIP Start (to DVI-1 & 3)	PP-HPSI-01 speed table control FCV-HPSI1-03, 04 100% open OV-SIS2,4-01 open	LPP + 28.29 s delay	SIP flow rate
Low Upper Downcomer Pressure (LUDP)		PT-DC_01 < 4.032 MPa	
SIT Begin (to DVI-1~4)	FCV-SIT1,2,3,4-01 100% open OV-SIS1,3-01 open	LUDP + 0.0 s delay	SIT flow rate
SIT Low Flow Conversion	FCV-SIT1,2,3,4-01: 18, 13, 24, 13% open	LT-SIT-1,2,3,4-01 < 72.8, 72.6, 72.0, 72.1%	LT-SIT-1,2,3,4-01 < 4.077, 4.066, 4.033, 4.039m
SIT Stop	FCV-SIT1,2,3,4-01: close	LT-SIT-1,2,3,4-01 < 47.4, 47.2, 46.6, 46.7%	LT-SIT-1,2,3,4-01 < 2.654, 2.643, 2.611, 2.66m
Core Shutdown			Core power off
DAS End			Data backup
System Cool-down			Follow the cool-down procedure

Table 6. Actual Sequence of Events of the SB-CL-09

Event	SB-CL-09 (seconds)
Test Start	0.0
LPP	24.0
Reactor Coastdown	24.4
2^{ry} System Isolation	31.0
SIP	52.0
LSC LSC at	196.0 IL-1A/-2B
SIT	445.0
Remarks	APR1400 6” CL Break

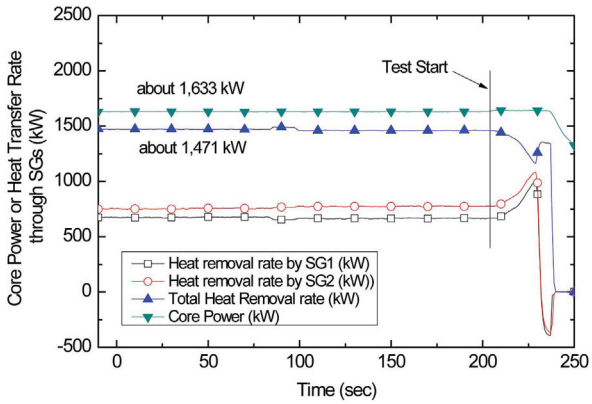

Fig. 3. Calculated Heat Balance during the Initial Steady State of the SB-CL-09

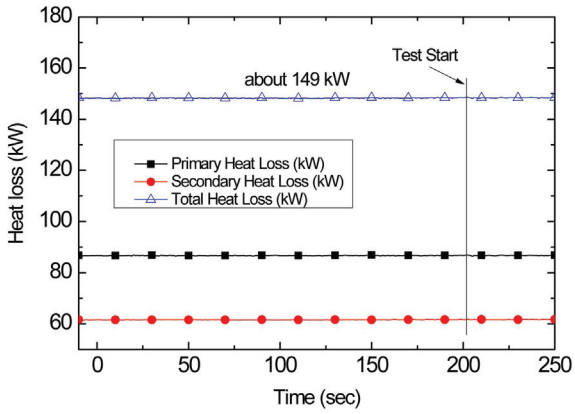

Fig. 4. Estimated Heat Loss Through the System of the SB-CL-09

descriptions on the phase separation during the cold leg break SBLOCA case can be found in the literature [10]. In this report, these five characteristic phases of SBLOCA will be described with the experimental results.

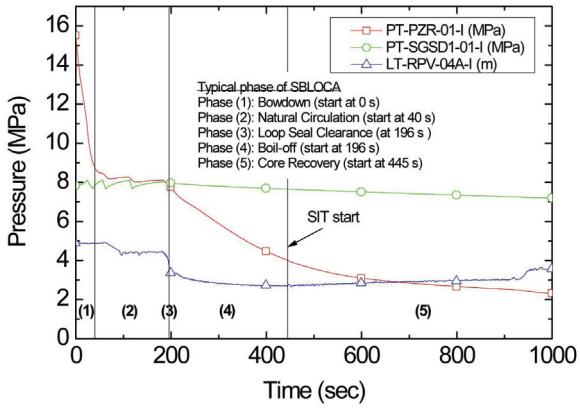

Fig. 5. Cold Leg SBLOCA Phase Separation in the SB-CL-09

The blowdown phase started with the opening of the break valve, OV-BS-06. Upon initiation of the break at the bottom of the cold-leg, the RCS primary side was rapidly depressurized until a flashing of the hot coolant into steam began. A reactor trip and an RCP trip were initiated by the low pressurizer pressure (LPP) setpoint of 10.72 MPa. Closure of the condenser steam dump valves isolated the SG secondary side. As a result, the SG secondary side pressure increased up to the main steam safety valve (MSSV) set point of 8.1 MPa, and steam was released through the MSSV. The ECCS actuation signal was also generated at the LPP signal with a time delay. In this phase, coolant in the RCS remained in the liquid phase. The rapid depressurization ended when the pressure fell to just above the saturation pressure of the SG secondary side. The break flow in the RCS was single-phase liquid throughout the blowdown period.

When the blowdown phase ended, a two-phase natural circulation phase was established in the RCS loops with the decay heat removed by a heat transfer (condensation and convection) to the SG secondary side. As more coolant was lost from the RCS through the break, steam accumulated in the downhill side of the SG U-tubes and the crossover leg. The natural circulation phase might continue until there is insufficient driving head on the cold leg side of the loops, owing to the accumulation of steam in loops between the top of the steam generator tubes and the loop seals. With the loop seals present, the break remained covered with water. The RCS water inventory continued to decrease and the steam volume in the RCS increased. The relative pressure in the core increased, which, together with the loss of coolant inventory through the break, caused liquid levels in the core and the SG to continue to decrease. The behavior of the collapsed water levels of the downcomer and the core region can be observed in Fig. 6, which shows that the core mixture level dropped below the top of the core. However, the cladding experienced no temperature excursion. A differential pressure between the downcomer and the upper head region (DP-DCUH1-01) reached its maximum value during this instant, as presented in Fig. 7.

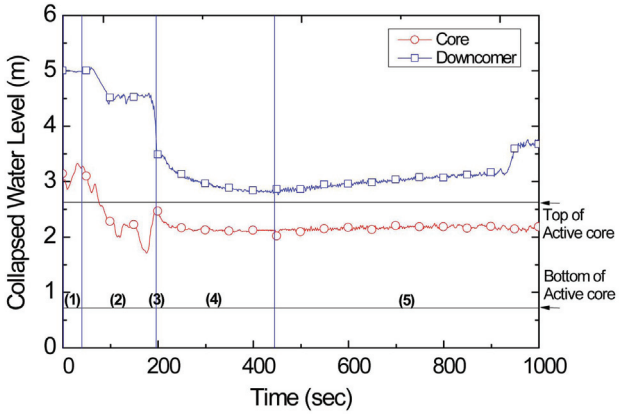

Fig. 6. Collapsed Water Levels of the Downcomer and the Core Region

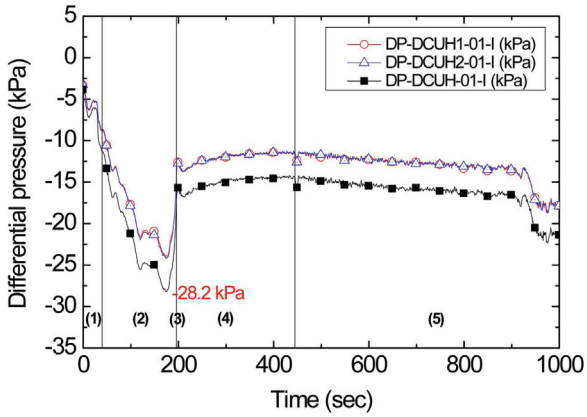

Fig. 7. Differential Pressure between the Downcomer and the Upper Head Region

When the liquid level of the downhill side of the SG was depressed to the elevation of the loop seals, the seals were cleared and steam in the RCS was vented to the cold legs. The break flow changed from a low quality mixture into primarily steam. This relieved the back-pressure in the core, and the core liquid level was restored to the cold leg elevation by a flow from the downcomer.

After the loop seal clearance, the RCS primary side pressure started to decrease below that of the secondary side, as can be seen in Fig. 5. This is mainly due to the increase of the break flow quality, resulting in a lower mass flow rate but a higher volumetric flow through the break. The collapsed water (or mixture) levels of the downcomer and the core region decreased a little bit as a result of the core boiling in this phase. This is due to the fact that the RCS pressure is too high for the safety injection from the SIT to make up for the boil-off rate.

The core recovery phase started with the instant of SIT injection. The vessel mass inventory increased and the core recovery was established, as can be observed in Fig. 6. In a small break LOCA case, the SIT injection into the RPV starts before the reactor coolant is completely

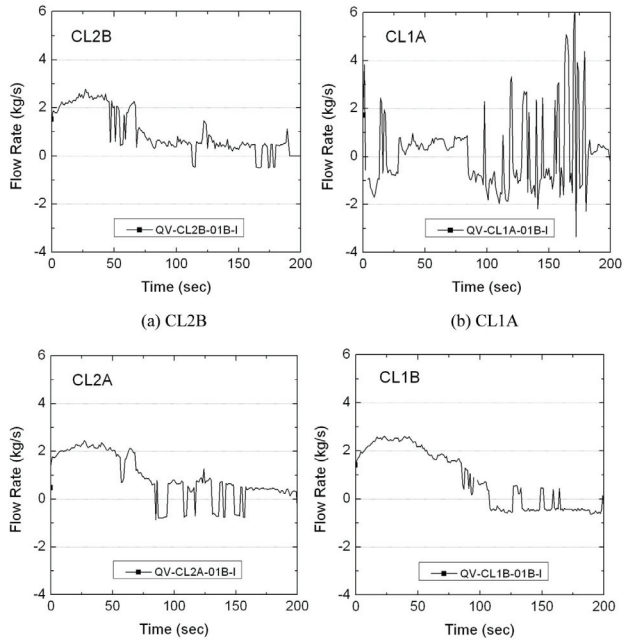

(a) CL2B (b) CL1A

Fig. 8. Cold leg Flow Direction during the SB-CL-09

discharged into the containment vessel, and the RCS pressure is still above the containment pressure.

The flow direction in the four cold legs during the present experiment can be observed in Fig. 8. With the opening of the break valve at 204 s, a reversed flow direction in cold leg-1A was observed. On the other hand, in the other cold legs, the flow rate was largely increased. This flow reversal in the broken cold leg and the flow rate increasing phenomena is typical for the cold leg break SBLOCA case. As can be seen in Fig. 8 (b), the flow rate in the broken cold leg (CL-1A) showed a very fluctuating nature. Moreover, from a more detailed observation, it can be observed that the flow direction in cold leg-1A was highly changeable with time.

3. COMPARISON OF CODE CALCULAITONS

The submitted transition calculation results were qualitatively compared with the measured data. All compared figures are included in Appendix A of reference 5. A qualitative prediction accuracy of the submitted calculations was discussed focusing on the important thermal-hydraulic parameters which have high relevance to safety, e.g. pressure and differential pressure, loop fluid temperature, downcomer fluid temperature, downcomer water level, core water level, loop seal clearing, etc., as described in section 5.3 of reference 5.

It is noteworthy that a CPU time comparison is discussed in this section. The CPU time and the time step were requested to examine the calculation performance of the submitted

calculations. The actual CPU time until 1,600 s and time step at 1,600 s are tabulated in Table 7. A great difference in the CPU time was found among the calculations. Participants B1 and B4 showed the fastest calculation time among the participants, while participants B3, C1, and C3 showed the latest calculation time. The time step during the calculation was also requested to investigate the calculation performance. The time step did not show a significant variation during the whole calculation time. Participant B3 had a minimum time step of 0.001 s. Participants A1 and A3 had a maximum time step of 0.01 second. The CPU time was the shortest for participants A2, B1, B2, B4 and C2 when the time step varied around 0.034 seconds.

4. DISCUSSION ON KEY THERMAL HYDRAULIC PHENOMENA

4.1 Two-phase Break Flow

The break flow rate is one of the most important boundary conditions for the test simulation. It is considered that choking occurs during the discharge of the single-phase liquid, two-phase mixture, and the single-phase steam throughout the test. In the ATLAS facility, the total break flow rate were was calculated using the experimental data of QV-CS-03, LC-CS-01, and LC-CS-02, and as a complementary method to the load cell-based break flow measuring method, a RCS inventory-based break flow estimation method has also been applied. From all the participants' predictions, the break flow is high and fluctuating during the earlier stage at up to 174 s, decreases rapidly, and maintains a low and steadier flow thereafter during the DSP-02 test.

As a ratio of the downstream to the upstream pressures of the break spool piece decreased up to 0.2, it was presumed that a choking flow was maintained throughout the test. A subcooled liquid choking flow was observed in the earlier period of the test, and then rapidly converted into a saturated two-phase choking flow. After it maintained a short duration, the two-phase choking was changed into a single-phase steam choking flow after around 174 s, and maintained a single-phase choking condition during the remaining test period of the DSP-02 test.

Generally the break flow rate decreased rapidly after the break, reached a plateau with a short duration, and then decreased again in every simulation. Most of the simulation results showed the trends of subcooled liquid choking, saturated two-phase choking, and single-phase steam choking. However, there are some differences case by case. A1, A2, and A3 of Group A, B2 and B4 of Group B, and C1, C2, C3, and C4 of Group C predicted the experimental break flow rates well, but B1 and B4 of Group B under-predicted the experimental data during the whole period.

Table 8 shows a brief summary of the break flow rate and accumulated mass. The peak flow rate, mean flow rate at the plateau, transition time from the two-phase to single-phase flow, and the accumulated masses at the transition time and at 1,600 s were compared with the experimental data. The MARS and RELAP5 code has modified Henry-Faukse critical flow models. The reported critical flow models are listed in Table 8, including the discharge coefficient used to fit their simulation results to the experimental data. The reported discharge coefficients were between 0.80 and 0.93.

Table 7. CPU Time and Time Step

No.	Group	Participants[1)]	CPU time (s) until 1,600 s	Time step (s)	Remark
1	A	A1	1345.42	0.01	
2		A2	569.00	~0.034	
3		A3	1,376.62	0.01	
4	B	B1	503.14	~0.034	
5		B2	638.48	~0.034	until 1500 s
6		B3	4191.62	0.001	
7		B4	509.59	~0.034	
8	C	C1	3,951.00	~0.034	until 596 s
9		C2	680.64	~0.034	
10		C3	7,623.53	~0.002	
11		C4	1,284.86	~0.034	

Note 1) All the participants are divided into 3 groups as A1 through A3, B1 through B4, and C1 through C4, respectively. Hereinafter, all the participants are described anonymously.

4.2 Downcomer Fluid Temperature Comparison

For a review of the downcomer fluid temperature, there are six subsections for each elevations from elevation 1 to elevation 6 azimuthally and in one section, for elevation 7. Please refer to the definitions of the elevations and azimuthal subsections in Figs. 9 and 10, respectively.

Most of the predictions showed that there were some multi-dimensional effects along the vertical elevation and the azimuthal direction. In this section, the multi-dimensional effects were considered according to the azimuthal direction for each level in the downcomer and vertical direction for specific subsections. There was just one piece of data for elevation 7, i.e., lumped data, and thus was not considered for the azimuthal effect.

The test data and participant predictions show similar trends with acceptable deviations for lower elevations, e.g., from elevation 1 to elevation 4. For higher elevations, e.g., from elevation 5 to elevation 7, there are quite large deviations between the test data and participants predictions. From the RPV downcomer level data, e.g., Figure A.119 of reference 5, most of the data remains above the top of the active core, e.g. ~2.7m, during the transient except that some predictions go to just below the top of the active core during 300~500 seconds and then return to higher elevations. For lower elevations, e.g., from elevation 1 to elevation 4, the downcomer temperature does not have much effect from the incoming ECC water due to pre-

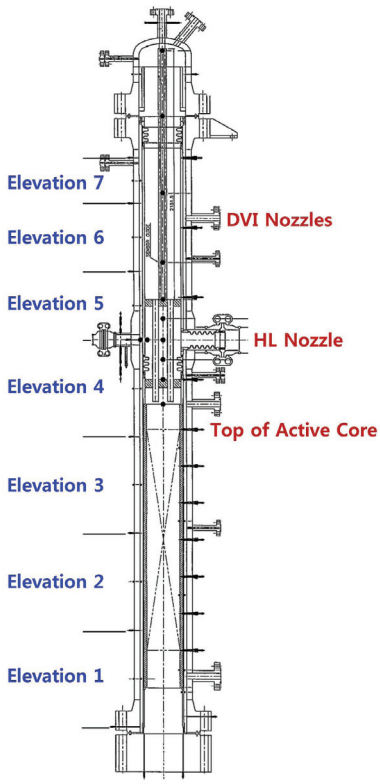

Fig. 9. Definition of the Elevation Numbers in the Downcomer for Comparison

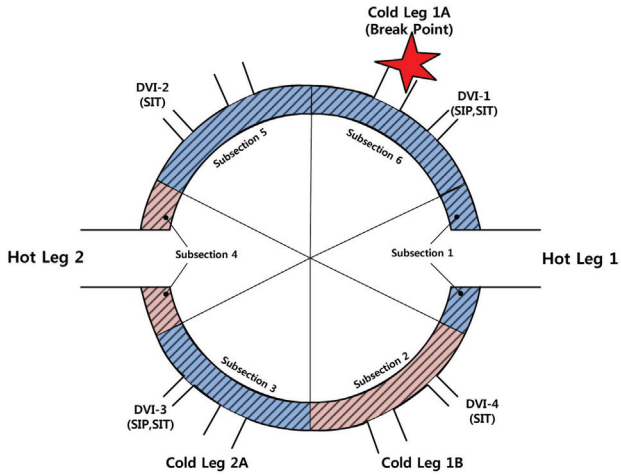

Fig. 10. Definition of Azimuthal Subsections in the Downcomer for Comparison

Table 8. Summary of the Break Flow Rate and Accumulated Mass

	Exp. (s)	Group A			Group B				Group C			
		A1	A2	A3	B1	B2	B3	B4	C1	C2	C3	C4
Peak flow rate	7.03	7.47	7.46	8.11	8.42	7.78	7.45	7.69	5.97	8.26	8.82	8.54
Mean flow rate at the plateau	4.54	3.85	3.88	3.82	4.04	3.87	4.14	3.81	4.17	3.94	4.50	4.07
Transition end time	176	168	188	176	163	172	158	195	174	181	149	156
Mass at transition time	825.6	765.1	786.2	800.9	717.4	781.5	779.9	812.5	766.4	804.8	773.5	735.9
Mass at 1,600 s	1723.7	1636.5	1636.2	1666.3	1752.1	1574.3 [2)]	1886.8	1769.2	1140.3 [3)]	1651.5	1720.2	1693.4
Critical flow model used	-	H-F [1)] Cd: 0.85	H-F [1)] Cd: 0.80	H-F [1)] Cd: 0.85	H-F [1)] Cd: NA	H-F [1)] Cd: 0.85	H-F [1)] Cd: NA	H-F [1)] Cd: 0.84	H-F [1)] Cd: 0.93	H-F [1)] Cd: 0.87	H-F [1)] Cd: 0.85 [4)]	H-F [1)] Cd: 0.90

[1)] Henry-Fauske Model, [2)] at 1,500 s, [3)] at 596 s, [4)] Recommended Cd = 0.9

existing relatively hot water. But at higher elevations, e.g., from elevation 5 to elevation 7, the downcomer temperatures are mainly affected by the incoming ECC water because there were just steam regions for higher elevations. The top of the active core is included in elevation 4 of the downcomer, which is why most of the temperature data shows different trends below and above elevation 4.

As in a typical SBLOCA scenario, the PZR pressure of the test followed a general trend. As shown in Fig. 11, the general trend of the PZR pressure of ATLAS and all participants' predictions can be split into 3 regions, e.g. initial blowdown, pressure plateau, and boil-off. In general, a boil-off will be triggered by the occurrence of the loop seal clearing(s), as shown in the figure. From the overall review of the test data and all predictions, certain common trends of the fluid temperature variations in the downcomer were found according to the 3 regions.

In review of the azimuthal effect, most of the predictions showed that there were two stages that represented the occurrence of a multi-dimensional effect, e.g., the initial stage and after SIT injection. For example, Fig. 12 showed these kinds of aspects in the SNU's calculation (e.g. elevation 4). (In the DSP-02 exercise, SNU performed a sensitivity calculation for the 2-dimensional behavior in the downcomer as remarked in Table 1.) As shown in the figure, most of the data for the initial stage looked to be affected by the actuation of the safety injection pump to a certain extent. After the loop seal clearing until SIT actuation, there are few azimuthal effects, which means a governing of the boil-off. But for the SIT injection stage, most of data predictions showed less relation to the actuation of the safety injection tanks. For a higher level, e.g., elevation 5, most of the data predictions were different from those of elevation 4 as shown in Fig. 13. For a comparison between the test data and predictions, test data for elevations 4 and 5 are shown in Fig. 14 and Fig. 15, respectively. From both figures, the initial stage shows quite a larger azimuthal effect than the predictions, but for the SIT injection, less azimuthal effects than the predictions. The test data of elevation 6 shows quite a large effect on the azimuthal direction for after the initial stage due to SIP and SIT injections as shown Fig. 16.

In the review of the vertical direction, the first 60 seconds from the break corresponded to the 'blowdown' region. In

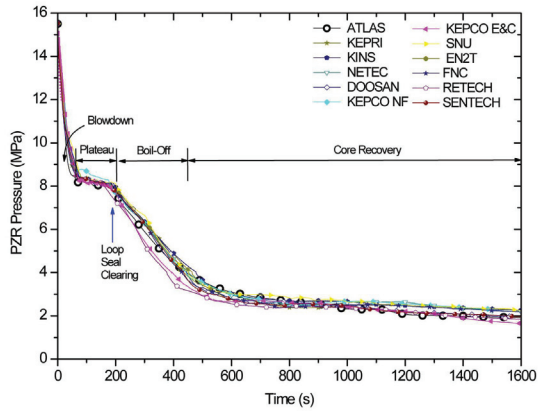

Fig. 11. Pressurizer Pressure of the ATLAS and all the Participants

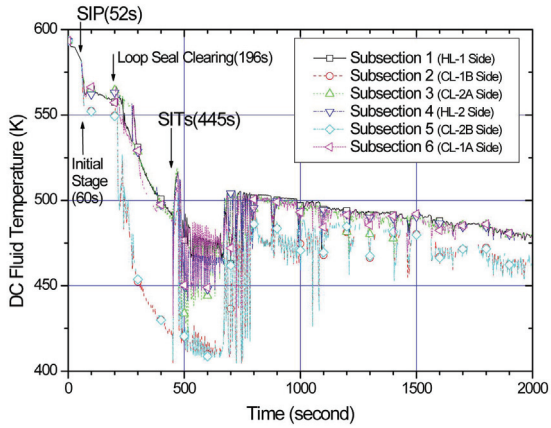

Fig. 13. Multi-Dimensional Effect for Azimuthal Direction (SNU, Elevation 5)

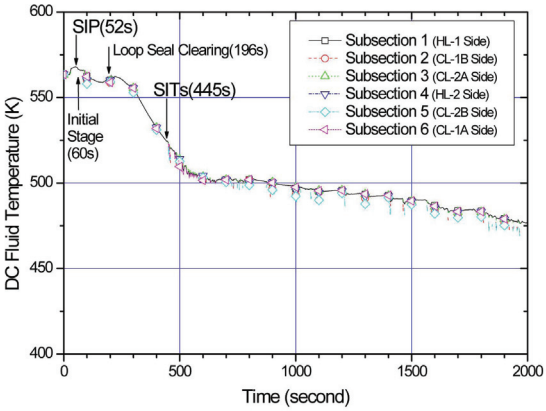

Fig. 12. Multi-Dimensional Effect for Azimuthal Direction (SNU, Elevation 4)

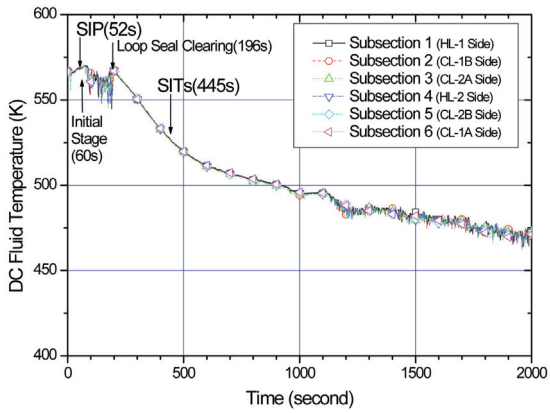

Fig. 14. Multi-Dimensional Effect for Azimuthal Direction (ATLAS, Elevation 4)

this region, most of the fluid temperatures in the downcomer decreased sharply just after the break, and then recovered to a certain value at the end of the blowdown region, as shown in Figs. 17 and 18. The 'pressure plateau' region remained from 60 seconds to 200 seconds.

As shown in Figs. 17 and 18, when the system pressure reached at the 'plateau' region, the fluid temperatures varied with respect to the vertical downcomer elevation. For example, in lower elevations 1 and 2, the fluid temperatures decreased slowly until the middle of the plateau and then increased to a certain value at the end of the plateau. But at the higher elevations 5 and 6, the fluid temperatures showed quite large oscillations, especially to lower values during the period of the plateau. Also, at middle elevations 3 and 4, the fluid temperatures showed intermediate trends, but close to those of the lower elevations. The oscillations of the fluid temperatures can be due to the actuation of the safety injection pump at 55 seconds. This was just before the entrance of the plateau. It can be concluded that the fluid temperatures in the higher downcomer elevations were affected by the cold ECC water from the safety injection pump. The loop seal clearings occurred at the intermediate leg 1A and 2B at 196 seconds, e.g., just before the end of the plateau. The test data showed that the oscillations became smaller at the loop seal clearings. When the system reached at the end of the plateau, most of the fluid temperatures came to concentrate at certain values.

It is noteworthy that the fluid temperature of the elevation 7 maintained the highest values for the blowdown and plateau regions. From the collapsed water level data, it was quickly depleted during the blowdown period at elevation 7, and since then no water level was detected. Thus, the steam at elevation 7 would have some effect from the hot vessel wall, e.g., wall heat transfer effect. This seems to be the reason why its temperature was always higher than the others'. These trends can be seen in Figs. 17 and 18.

When the system pressure reached the entrance of the boil-off region, e.g., at 200 seconds, most of the fluid temperatures showed nearly the same values, and then decreased according to the system pressure changes until 446 seconds, as shown in Fig. 19 and 20. After that, the temperature of elevation 7 showed quite large oscillations, especially to higher values until the end of the test. As mentioned before, there was no water at elevation 7, and

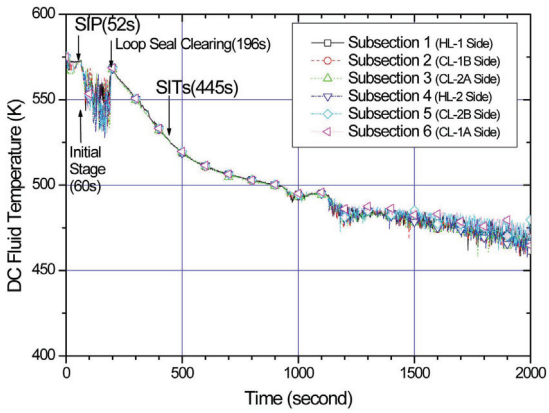

Fig. 15. Multi-Dimensional Effect for Azimuthal Direction (ATLAS, Elevation 5)

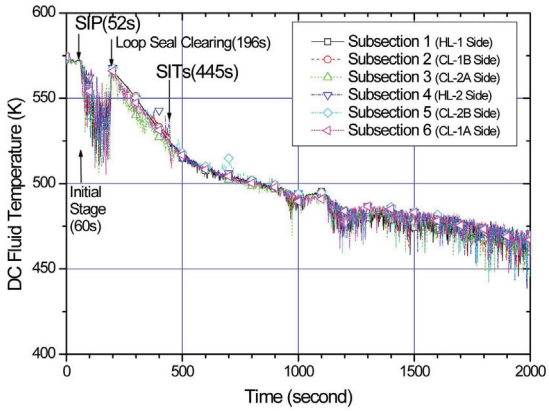

Fig. 16. Multi-Dimensional Effect for Azimuthal Direction (ATLAS, Elevation 6)

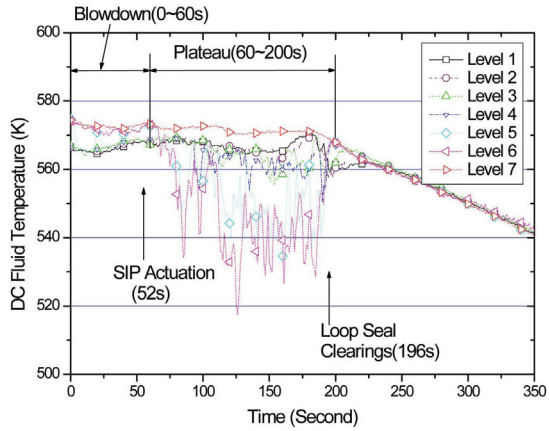

Fig. 17. Fluid temperature Distributions for Blowdown and Plateau Regions (ATLAS, Subsection 2)

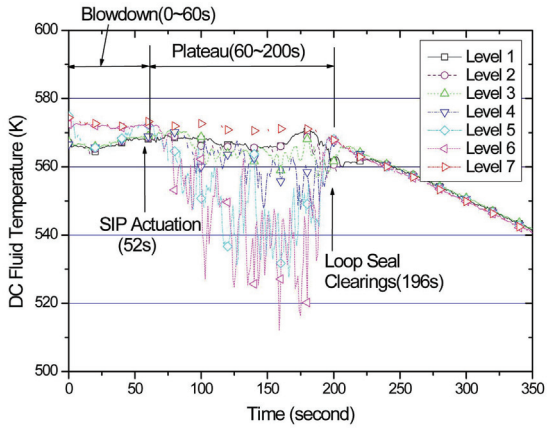

Fig. 18. Fluid Temperature Distributions for Blowdown and Plateau Regions (ATLAS, Subsection 4)

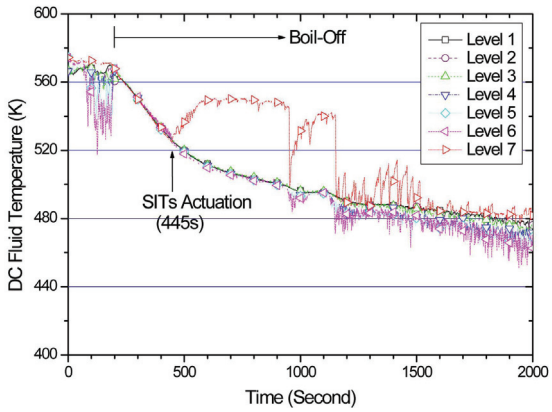

Fig. 19. Fluid Temperature Distributions for Boil-off Region (ATLAS, Subsection 2)

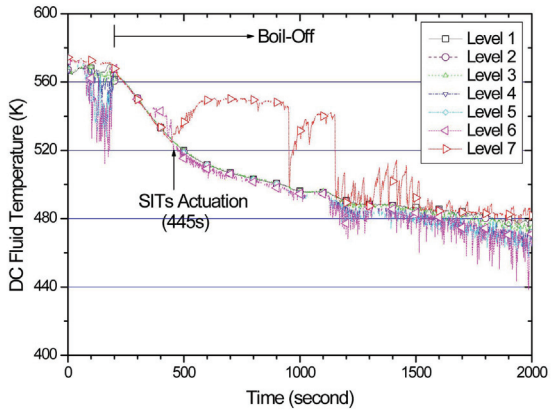

Fig. 20. Fluid Temperature Distributions for Boil-off Region (ATLAS, Subsection 4)

thus its temperature would be influenced by the wall heat transfer and showed the highest temperature. For the other elevations, the trends of the fluid temperatures between 2 subsections became different. In subsection 2 (refer to Fig. 19), all fluid temperatures in elevations 1 through 3 showed similar trends and values like a single curve. In subsection 4 (refer to Fig. 20), most of the fluid temperatures at elevations 1 through 3 showed similar trends and values like a single curve, as in subsection 2. But the temperatures in elevations 4 through 6 showed some oscillations, especially to lower values. This is because of the effect of the ECC water from the safety injection tanks, which actuated at 446 seconds. But in subsection 2, there was no evidence of the effect of the ECC water from the safety injection tanks.

4.3 Non-uniform Loop Seal Clearing

Unlike the LBLOCA, the loop seal clearing phenomena during the SBLOCA, especially for the cold-leg break situation, entirely governs the whole thermal-hydraulic behavior of the primary system. For the APR1400, four intermediate legs exist between the two SGs and four RCPs. In the SB-CL-09, a 6 inch cold-leg break was simulated. Generally, for the cold-leg SBLOCA case, the pressure of the upper-head region would be increased mainly due to the accumulated steam and water inventory in the upper-plenum. This built-up pressure acts as a suppression force to the core water level and resultantly the core water level will decrease possibly up to and/or below the top of the active core region. Simultaneously, the downcomer water level would increase due to the evacuated water inventory from the lower part of the core region.

This unbalanced hydro-static pressure between the core and the downcomer region acts as a potential pushing force to the SG side intermediate leg. The potential pushing force will be increased with time to overcome the hydro-static head in the intermediate leg. The unbalanced hydro-static pressure finally can be dissolved with the occurrence of the loop seal clearing. Therefore, the loop seal clearing phenomena is very important with respect to the PCT, one of the most important parameters to insure the safety of the reactor system.

The loop seal clearing behavior is closely related to the break location and the break size. Usually, a loop seal of the break loop is cleared first, and the number of cleared loop seals is dependent on the break size. The larger the break size is, the more the loop seal is cleared, as can be observed in Fig. 21 and 22, which show a collapsed water level behavior during the SB-CL-01 (4 inch cold leg SBLOCA test) and SB-CL-03 (8 inch cold leg SBLOCA test), respectively. This different loop seal clearing behavior with respect to the break size is mainly dependent on the unbalanced hydro-static pressure between the upper head and the downcomer region, as shown in Figs. 23 and 24 for SB-CL-01 and SB-CL-03, respectively. On the other hand, in the SB-CL-02, intermediate leg-1A and -2B were cleared.

4.4 Secondary Pressure

While the prediction of the primary system pressure was quite good, the secondary system pressures were not properly estimated in many calculations. In particular, the secondary system pressures subsequent to the MSSV opening were over-predicted. Only the calculations performed by participants B2 and A3 showed reasonable prediction performance of the secondary system pressures during the late phase calculation times after the MSSV opening. The reasons for the over-prediction of the secondary system pressure are complex. The secondary system pressure can be affected by the loop seal clearing behavior, the heat loss, and the fluid condition inside the U-tubes. In the calculations where the loop seal clearing behavior was not correctly predicted, the secondary system pressures show a tendency to be over-estimated. After the loop seal clearing, the U-tubes of the steam generators were emptied. However, if the loop seal was formed and not cleared in the intermediate legs, the reverse heat transfer in the U-tubes resulted in a heat up of the fluid inside the U-tubes, consequently causing an increase in the secondary system pressure.

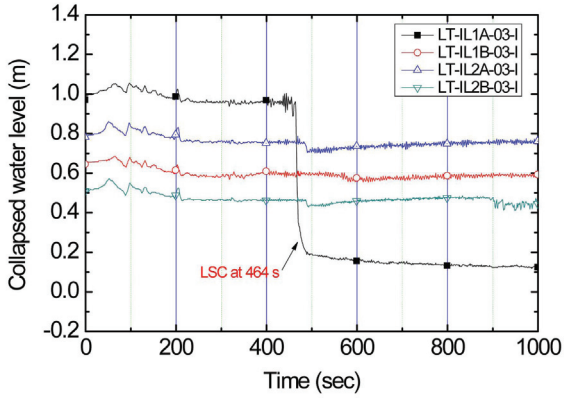

Fig. 21. Collapsed Water Level of Intermediate Leg during the SB-CL-01 (4-inch CL SBLOCA Test)

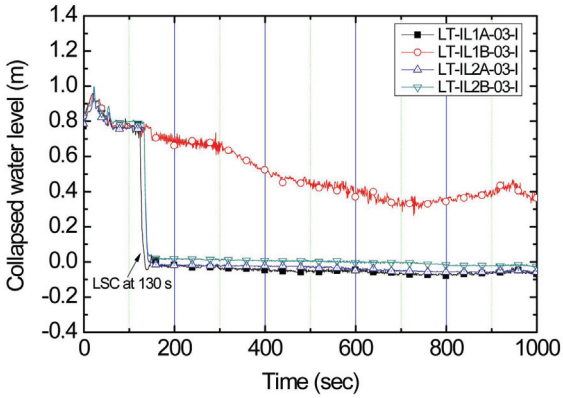

Fig. 22. Collapsed Water Level of Intermediate Leg during the SB-CL-03 (8-inch CL SBLOCA Test)

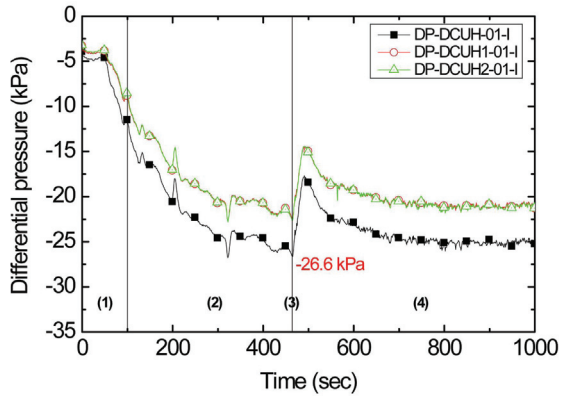

Fig. 23. Differential Pressure during the SB-CL-01 (4-inch CL SBLOCA Test)

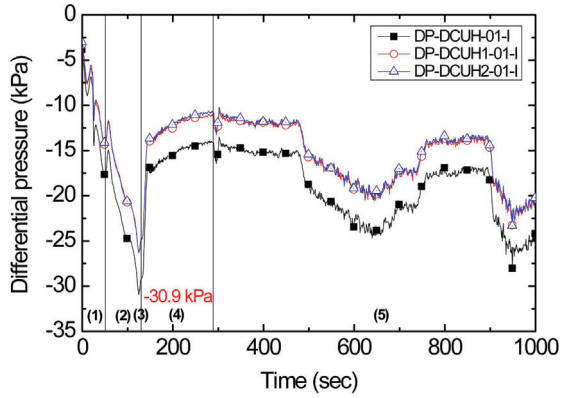

Fig. 24. Differential Pressure during the SB-CL-03 (8-inch CL SBLOCA Test)

In the SB-CL-09 test, the primary heat loss at the initial condition was about 66 kW and the secondary heat loss of each steam generator was about 28.5 kW. During the test, the primary heat loss was compensated by adding it to the core decay power table with respect to time. The secondary heat loss, however, was not compensated in the test. Table 9 summarizes the detailed heat loss modeling and the prediction performance of the secondary system pressure in each calculation. As for the primary heat loss, most calculations considered the primary heat loss by subtracting the constant heat loss from the initial core power. The modeling of the secondary heat loss, however, was differently applied to the participant's calculations as shown in Table 9. At this stage, a definite conclusion on the relation between the heat loss modeling and the secondary system pressure prediction cannot be made owing to a lack of detailed information on the code input modeling and the use of the different codes in each calculation. However, it can be rationally expected that modeling of the heat loss at the steam generators affects the secondary system pressure behavior. Participant C4 performed a sensitivity calculation for the effect of secondary heat loss on the secondary system pressure behavior. In the calculation where the secondary heat loss was considered, the secondary system pressure presented a similar trend with the SB-CL-09 test data. Despite the difference from a quantitative point of view, it can be found in the participant C4's calculation result that the heat loss at the steam generators needs to be properly modeled for the accurate estimation of the secondary system pressures.

Another possible source of over-prediction of the secondary pressure is the quality of the steam entering the U-tubes after the loop seal clearing. If the steam quality at the U-tube inlet is lower in the calculation than in the test, it would result in less reverse heat transfer from the secondary to the primary system and consequently higher secondary pressure than the data is obtained in the calculation and vice versa. Unfortunately, however, the present SB-CL-09 test does not provide such detailed local information on the steam quality to support this reasoning.

4.5 Major Findings from the Special Code Assessment

In the DSP-exercise, most of the participants adopted the MARS-KS code for open calculation, which is why special code assessments could be performed by the participants. In this section, the major findings from those activities are summarized as follows:

Table 9. Detailed Heat Loss Modeling and the Prediction Performance of the Secondary System Pressure in Each Calculation

Group	Participant	Detailed heat loss modeling		SG pressure prediction performance
		Primary system	Secondary system	
A	A1	Use of reduced core power	N/A	Overestimation
	A2	Use of reduced core power	N/A	Overestimation
	A3	N/A	Constant value: 24.5 kW/SG	Slightly under-estimation
B	B1	No information	No information	Overestimation
	B2	N/A	N/A	Good agreement
	B3	Use of reduced core power	N/A	Overestimation
	B4	Use of reduced core power	No information	Overestimation
C	C1	Use of reduced core power	Constant value: 24.6 kW/SG	Overestimation
	C2	Use of reduced core power	No information	Overestimation
	C3	No information	No information	Overestimation
	C4	Use of reduced core power	N/A	Overestimation

(1) Break flow modeling;

It was found that detailed upstream modeling from the break nozzle to the break valve resulted in better agreement with the data. In such a detailed modeling, the discharge coefficient of Cd=1.0 is recommended as one of the user guidelines.

(2) Loop seal clearing;

Most participants were not successful in reproducing asymmetric loop seal clearing behavior. The loop seal clearing was greatly affected by a small model change. From the viewpoint of safety, where the loop seal clearing occurred and how many loops were cleared seem to be unimportant. However, the occurrence timing is very important because it governs the event progress since then.

(3) ECC bypass rate;

This was estimated by injecting boron during the code calculation by one participant, who tried a creative calculation method. Around a 30%-45% ECC bypass rate was obtained. However, this bypass rate needs to be confirmed by experimental data. Unfortunately, experimental evidence to confirm the estimated ECC bypass rate is not available. This finding can be feedback to experimentalists to improve the measurement methodology.

(4) Heat loss effects;

A detailed sensitivity study was done to answer the question why the secondary pressure was over-predicted by almost all calculations. It was found that such over-predictions of the secondary pressure were due to a lack of heat loss modeling in the secondary system. The effects of heat loss were included in the model, and a very nice agreement with the data was obtained.

(5) Momentum effects of ECC water;

This was not a dominant factor affecting the transient calculations.

(6) 2D behavior;

Practical 2-D behavior was observed in the ATLAS experiment. In particular, fluid mixing was not properly predicted by most calculations. A cross junction k-factor was not helpful to resolve insufficient mixing. The use of a turbulent mixing model of the MARS-3D code is recommended for better prediction.

(7) ACC component;

The accumulator component needs to be improved to remove the initial peak and minimize the flow oscillation. When a simple PIPE component is used to model the SITs instead of the ACC component, the initial peak and flow oscillation can be avoided.

(8) Condensation;

Injection of cold water into the downcomer results in excessive condensation, causing an increase in the downcomer water level and a decrease in the core water level. It was found that utilizing the ECC mixer model mitigated the condensation. The condensation model needs improvement.

(9) RPV upper head temperature;

In most calculations, it was close to the hot leg temperature owing to a reverse downcomer-upper head bypass flow path. This caused early flashing and depression in the downcomer water level.

(10) High core water level before the loop seal clearing;

This was due to a high reverse flow from the steam generator to the RPV upper head. Appling the CCFL option to the RPV fuel assembly plate can mitigate this disagreement.

5. ACCURACY QUANTIFICATION

Compared to the DSP-01 exercise, the host organization adopted the BEMUSE phase 2 project methodology for accuracy quantification. The methodology of the accuracy quantification consists of (1) a global acceptability factor for the nodalization development, Q_A; (2) global acceptability factor for the nodalization qualification at the steady state level, Q_B; and (3) global accuracy quantification for the deviations between calculations and measurements quantified by FFTBM, AA_{tot}. In the quantification of the DSP-01, only this one was discussed in reference 2.

5.1 Nodalization Qualification (QA)

As the quality of transient code calculations is greatly dependent on how well the code model is initialized at a steady state condition, a steady state qualification based on measured data was performed, following the similar methodology as that proposed by the BEMUSE phase-2 program [11] in the present DSP-02. The steady state qualification includes two different steps: one is related to the evaluation of the geometrical data and of numerical values implemented in the nodalizations; the other is related to the quality of the steady state calculation results. Nine parameters have been selected for nodalization qualification as shown in Table 10.

As the first step, the acceptable errors (AE) for the quantification process were determined. Different AEs from 1% to 3% were used depending on the parameters shown in Table 10. The percentile error, E, was defined as the ratio

$$E = \frac{\left|(\exp value \pm \exp error) - calc\ value\right|}{\left|(\exp value \pm \exp error)\right|} \quad (3)$$

The percent error, E becomes zero if the calculated value is between the experimental lower and upper values, taking into account the experimental error.

Secondly, weighing factors taking into consideration the importance of the parameters with respect to the present SBLOCA transient were determined. Taking into account the phenomena of the SBLOCA, the relative importance of the secondary inventory was assumed to be half that of the primary inventory. Thus, weighting factors, W_i, of 1.0 and 0.5 were used for the primary and secondary inventory, respectively. The single acceptability factor, Q_{Ai} was then obtained by the following formula:

$$Q_{Ai} = \frac{E}{AE} \cdot W_i \quad (4)$$

where, normalized weighting factors were used. Finally, the global acceptability factor, Q_A, can be obtained by summing the whole single acceptability factors

$$Q_A = \sum_i Q_{Ai} \quad (5)$$

The effects of selected parameters on Q_{Ai} are shown in Fig. 25. All calculated Q_{Ai} are plotted together. The secondary circuit volume (parameter 2) and maximum axial power distribution for the average rod (parameter 9) showed the greatest values in Q_{Ai} among the others. Final nodalization quantification results are shown in Table 11.

Table 10. Parameters for Nodalization Quantification

No	Parameter	Unit	Acceptable Error (%)	Weighting Factor (WF)	Experiment (SB-CL-09)		Remarks
					Y_E	Error (±)	
1	Primary circuit volume	m^3	2%	1.0	1.6366	1%	Including PZR
2	Secondary circuit volume	m^3	2%	0.5	2.8385	2%	SGs~FCV-MSCV-01
3	Core heat structure surface area	m^2	2%	1.0	22.2	0.44	Active Core
4	SG U-tubes heat structure external surface area (without tube sheet)		2%	0.5	69.2	1.38	
5	SG U-tubes heat structure internal surface area (without tube sheet)		2%	0.5	58.5	1.17	
6	Core heat structure volume	m^3	3%	1.0	5.27E-02	1.6E-03	Active Core
7	SG U-tubes heat structure volume (without tube sheet)		3%	0.5	7.03E-02	2.1E-03	
8	Average of the axial power distribution for the average rod in average channel (group 1~3)	kW/m	1%	0.5	2.2	0.02	
9	Maximum of the axial power distribution for the average rod in average channel (group 1~3)	kW/m	1%	1.0	3.2	0.03	

In the literature [11], Q_A<1.0 is required as an acceptable criterion. Around 50% of the calculations fulfilled the global acceptability in the present exercise. In fact, Q_A is affected by two factors, AE and W_i, and a proper choice of those factors are important for a meaningful quantification process. In the present quantification, two factors were determined by considering the relative importance of each inventory during the typical SBLOCA scenario, though they look more or less subjective. From Table 11, participant B4 showed the best result of 0.585, and participant C4 showed the greatest value of 2.14 among the participants.

5.2 Steady State Qualification (Q_B)

Steady state results can be quantified by using the similar methodology used in the quantification of QA in the previous section. For the quality of the steady state calculation results, 21 parameters have been selected for a steady state qualification, as shown in Table 12.

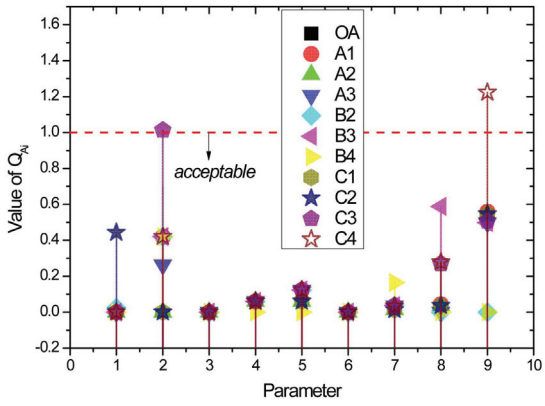

Fig. 25. Effects of Parameters on Q_{Ai}

At first, the acceptable errors (AE) for the quantification process were determined. Taking into account the measurement uncertainties, different AEs from 0.25% to 30% were used depending on the parameters shown in Table 12. The percentile error, E, was defined as Eq. (3).

Secondly, weighing factors taking into consideration the importance of the parameters with respect to the present SBLOCA transient were determined, as shown in Table 12. Also, the single acceptability factor, Q_{Bi}, was obtained by Eq. (4). Finally, the global acceptability factor, Q_B, can be obtained by summing the whole single acceptability factors as in Eq. (5). Calculated results for the submitted calculations are summarized in Table 13.

In the literature [11], Q_A<1.0 is required as an acceptable criterion. Only 2 calculations fulfilled the global acceptability in the present exercise. From Table 13, participant A2 showed the best result of 0.159, and participant C2 showed the greatest value of 3.058 among the participants.

5.3 FFTBM Methodology

Application of FFTBM to the present DSP-02 calculation was performed to evaluate the accuracy of the submitted calculation results. As in the DSP-01 exercise, 22 parameters have been used to characterize all the relevant phenomena that were measured during the test, as shown in Table 7 of reference 2. Also, the weighting factors were used to consider the different importance from the viewpoint of a safety analysis and to calculate the overall accuracy of the calculation, i.e., the total average amplitude (AA_{tot}). In the present analysis, the weighting factors used in Table 7 of reference 2 were adopted.

For the quantification of each participant's calculation, three cases with different time frames were evaluated as shown in Table 14. In the first time frame between 0 s to

Table 11. Nodalization Qualification Results

Parameters (Q_{Ai})	OA	Group A			Group B			Group C			
		A1	A2	A3	B2	B3	B4	C1	C2	C3	C4
1	0.000	0.000	0.000	0.000	0.023	0.000	0.000	0.000	0.444	0.000	0.000
2	0.000	0.421	0.000	0.264	0.421	0.421	0.421	0.000	0.000	1.013	0.421
3	0.000	0.000	0.000	0.000	0.000	0.000	0.000	0.000	0.000	0.000	0.000
4	0.060	0.060	0.060	0.060	0.060	0.060	0.000	0.060	0.060	0.060	0.060
5	0.060	0.124	0.060	0.124	0.123	0.123	0.000	0.060	0.060	0.123	0.124
6	0.000	0.000	0.000	0.000	0.000	0.000	0.000	0.000	0.000	0.000	0.000
7	0.013	0.036	0.013	0.036	0.037	0.037	0.164	0.013	0.013	0.036	0.033
8	0.036	0.045	0.036	0.000	0.000	0.588	0.000	0.036	0.036	0.271	0.279
9	0.546	0.559	0.546	0.498	0.000	0.498	0.000	0.546	0.546	0.507	1.223
Q_A	**0.716**	**1.244**	**0.716**	**0.981**	**0.664**	**1.727**	**0.585**	**0.716**	**1.160**	**2.009**	**2.140**

Table 12. Parameters for Steady State Quantification

No	Parameter	Acceptable Error (%)	Weighting Factor (WF)	Experiment (SB-CL-09)	
				Y_E	Error (±)
Primary system					
1	- Core power (MW)	2	0.80	1.633	0.033
2	- Heat loss (kW)	3	0.50	66	1.98
3	- PZR Pressure (MPa)	0.25	1.00	15.5	0.04
4	- Hot leg temp. (K)	0.5	0.60	597.7	2.4
		0.5	0.60	598.7	2.4
5	- Cold leg temp. (K)	0.5	0.60	565.4	2.4
		0.5	0.60	565.5	2.4
		0.5	0.60	564.2	2.4
		0.5	0.60	565.3	2.4
6	- RCS flow rate (kg/s)	15	0.40	2.02	0.30
		15	0.40	1.84	0.28
		15	0.40	1.89	0.28
		15	0.40	1.97	0.30
7	- Core bypass flow rate (kg/s)	30	0.50	0.04	0.01
		30	0.50	0.11	0.03
8	- Pressurizer level (m)	3.4	0.30	3.83	0.13
Secondary system					
9	- Dome Pressure (MPa)	0.25	1.00	7.82	0.02
		0.25	1.00	7.82	0.02
10	- Steam temp. (K)	0.5	1.00	566.9	2.4
		0.5	1.00	566.7	2.4
		0.5	1.00	568.5	2.4
		0.5	1.00	568.8	2.4
11	- FW temp. (K)	0.5	0.40	505.4	2.4
		0.5	0.40	506.4	2.4
		0.5	0.40	496.5	2.4
		0.5	0.40	495.7	2.4
12	- FW flow rate (kg/s)	1.5	0.40	0.373	0.006
		1.5	0.40	0.382	0.006
		1.5	0.40	0.044	0.001
		1.5	0.40	0.042	0.001
13	- Water level (m)	3.4	0.50	4.71	0.07
		3.4	0.50	5.03	0.07
14	- Circulation ratio (CR)	10	0.70	9.74	0.1
		10	0.70	9.67	0.1
15	- Heat removal (MW)	10	0.30	0.673	NA
		10	0.30	0.752	NA
16	- Heat loss (kW)	10	0.30	28.5	NA
		10	0.30	28.5	NA
ECCS					
17	- SIT pressure (MPa)	0.25	0.40	4.24	0.01
		0.25	0.40	4.15	0.01
		0.25	0.40	4.01	0.01
		0.25	0.40	4.17	0.01
18	- SIT temp. (K)	0.5	0.40	322.5	2.4
		0.5	0.40	323.2	2.4
		0.5	0.40	323.2	2.4
		0.5	0.40	325.4	2.4
19	- SIT level (m)	3.4	0.40	5.28	0.18
		3.4	0.40	5.32	0.18
		3.4	0.40	5.32	0.18
		3.4	0.40	5.32	0.18
20	- RWT temp. (K)	0.5	0.20	323.2	2.4
Containment					
21	- Pressure (MPa)	0.25	0.01	0.1013	0.0002

Table 13. Steady State Quantification Results

No	Parameter	OA	A1	A2	A3	B2	B3	B4	C1	C2	C3	C4
Primary system												
1	- Core power (MW)	0.054	0.033	0.000	0.000	0.000	0.000	0.000	0.054	0.033	0.033	0.033
2	- Heat loss (kW)	0.000	0.000	0.000	0.000	0.000	0.000	0.000	0.000	0.000	0.000	0.000
3	- PZR Pressure (MPa)	0.000	0.000	0.000	0.000	0.000	0.000	0.000	0.000	0.000	0.000	0.000
4	- Hot leg temp. (K)	0.000	0.000	0.000	0.000	0.000	0.000	0.000	0.000	0.000	0.000	0.000
		0.000	0.000	0.002	0.000	0.000	0.000	0.000	0.000	0.000	0.000	0.000
5	- Cold leg temp. (K)	0.002	0.001	0.001	0.001	0.000	0.000	0.002	0.002	0.002	0.002	0.002
		0.003	0.002	0.002	0.002	0.000	0.000	0.003	0.003	0.003	0.003	0.003
		0.000	0.000	0.000	0.000	0.000	0.000	0.000	0.000	0.000	0.000	0.000
		0.001	0.001	0.000	0.000	0.000	0.000	0.001	0.001	0.001	0.001	0.001
6	- RCS flow rate (kg/s)	0.000	0.000	0.000	0.000	0.000	0.000	0.000	0.000	0.000	0.000	0.000
		0.000	0.000	0.000	0.001	0.000	0.000	0.000	0.000	0.000	0.000	0.000
		0.000	0.000	0.000	0.000	0.000	0.000	0.000	0.000	0.000	0.000	0.000
		0.000	0.000	0.000	0.000	0.000	0.000	0.000	0.000	0.000	0.000	0.000
7	- Core bypass flow (kg/s)	0.113	0.083	0.000	0.067	0.109	0.109	0.117	0.113	0.109	0.111	0.013
		0.046	0.065	0.000	0.038	0.043	0.049	0.056	0.046	0.049	0.054	0.083
8	- Pressurizer level (m)	0.015	0.000	0.000	0.036	0.000	0.000	0.009	0.015	0.015	0.000	0.012
Secondary system												
9	- Dome Pressure (MPa)	0.000	0.000	0.000	0.016	0.000	0.460	0.000	0.000	0.000	0.000	0.000
		0.000	0.000	0.000	0.016	0.024	0.460	0.000	0.000	0.000	0.000	0.000
10	- Steam temp. (K)	0.000	0.000	0.000	0.000	0.000	0.000	0.000	0.000	0.039	0.000	0.000
		0.000	0.000	0.000	0.000	0.000	0.000	0.000	0.000	0.036	0.000	0.000
		0.000	0.000	0.000	0.010	0.000	0.000	0.000	0.000	0.060	0.000	0.000
		0.000	0.000	0.000	0.014	0.000	0.000	0.000	0.000	0.065	0.000	0.000
11	- FW temp. (K)	0.000	0.000	0.000	0.000	0.000	0.000	0.000	0.000	0.015	0.000	0.000
		0.000	0.000	0.000	0.000	0.000	0.000	0.000	0.000	0.021	0.000	0.000
		0.041	0.041	0.000	0.041	0.000	0.000	0.000	0.041	0.041	0.041	0.041
		0.046	0.046	0.000	0.046	0.000	0.000	0.000	0.046	0.046	0.046	0.046
12	- FW flow rate (kg/s)	0.058	0.057	0.060	0.065	0.094	0.058	0.000	0.058	0.055	0.057	0.057
		0.032	0.032	0.040	0.040	0.089	0.032	0.000	0.032	0.030	0.032	0.032
		0.000	0.000	0.000	0.037	0.000	0.049	0.000	0.000	0.023	0.000	0.000
		0.024	0.034	0.000	0.039	0.051	0.049	0.000	0.024	0.024	0.034	0.034
13	- Water level (m)	0.050	0.112	0.005	0.026	0.321	0.014	0.011	0.050	0.055	0.055	0.057
		0.008	0.147	0.042	0.000	0.342	0.007	0.039	0.008	0.014	0.013	0.015
14	- Circulation ratio (CR)	0.060	0.274	0.004	0.006	0.020	0.000	0.036	0.060	0.928	0.076	0.110
		0.057	0.274	0.003	0.004	0.028	0.000	0.029	0.057	0.888	0.072	0.107
15	- Heat removal (MW)	0.000	0.000	0.000	0.005	0.004	0.000	0.009	0.000	0.000	0.000	0.000
		0.000	0.000	0.000	0.005	0.006	0.000	0.008	0.000	0.000	0.000	0.000
16	- Heat loss (MW)	0.000	0.000	0.000	0.000	0.000	0.000	0.000	0.000	0.000	0.000	0.000
		0.000	0.000	0.000	0.000	0.000	0.000	0.000	0.000	0.000	0.000	0.000
ECCS												
17	- SIT pressure (MPa)	0.297	0.000	0.000	0.000	0.111	0.000	0.000	0.297	0.000	0.044	0.000
		0.167	0.106	0.000	0.106	0.000	0.000	0.000	0.167	0.106	0.060	0.106
		0.016	0.328	0.000	0.328	0.211	0.000	0.000	0.016	0.328	0.281	0.328
		0.196	0.075	0.000	0.075	0.008	0.000	0.000	0.196	0.075	0.030	0.075
18	- SIT temp. (K)	0.000	0.000	0.000	0.000	0.000	0.000	0.000	0.000	0.000	0.000	0.000
		0.000	0.000	0.000	0.000	0.000	0.000	0.000	0.000	0.000	0.000	0.000
		0.000	0.000	0.000	0.000	0.000	0.000	0.000	0.000	0.000	0.000	0.000
		0.010	0.000	0.000	0.000	0.000	0.000	0.000	0.010	0.000	0.000	0.000
19	- SIT level (m)	0.036	0.000	0.000	0.009	0.008	0.000	0.000	0.036	0.000	0.000	0.000
		0.039	0.000	0.000	0.006	0.005	0.000	0.000	0.039	0.000	0.000	0.000
		0.039	0.000	0.000	0.006	0.005	0.000	0.000	0.039	0.000	0.000	0.000
		0.039	0.000	0.000	0.006	0.005	0.000	0.000	0.039	0.000	0.000	0.000
20	- RWT temp. (K)	0.000	0.000	0.000	0.000	0.000	0.031	0.000	0.000	0.000	0.000	0.000
Containment												
21	- Pressure (MPa)	0.000	0.000	0.000	0.000	0.000	0.000	0.000	0.000	0.000	0.000	0.000
	Q_B	**1.449**	**1.712**	**0.159**	**1.050**	**1.484**	**1.318**	**0.319**	**1.449**	**3.058**	**1.046**	**1.153**

24 s, 19 parameters out of the selected 22 parameters were used because the SIP and SIT were not available during this period. The parameters relevant to the SIP and SIT were excluded in the FFTBM calculation. In the second time frame between 0 s to 440 s, the SIT was not activated in the test, and thus 2 parameters relevant to the SIT were excluded in the FFTBM calculation. In the whole time frame calculation, the 22 selected parameters were used to get the final AA_{tot}. For all cases, the cut-off frequency was set to 1.0 Hz.

A summary of the results of FFTBM application to the DSP-02 can be seen in Table 15. Overall, most calculations showed good prediction results except for participant B1's calculation. (In this report, the authors suggest a criteria for the accuracy of a given calculation, e.g., a 'good prediction' if $AA_{tot} < 0.5$; and a 'poor prediction' if $AA_{tot}t > 0.5$. The original categorization of the total AA_{tot} can be seen in reference 12.) This FFTBM was based on several assumptions; selection of variables, selection of the time frame of interest, weighting factors, and cut-off frequency. These assumptions were more subjective than objective so that the ranking among the calculations may be changed if different assumptions were used. Therefore, the ranking in Table 15 does not mean definite superiority of one calculation over the others. However, when the present assumptions were used, participant A2's calculation showed

Table 14. Selected Time Interval for the Present FFTBM Analysis

Time of interval	Phase relevant to PIRT	Phenomena Observed	Number of data	Max. frequency $f_{max} = 0.5\ f_s$ (Hz)
0~24 s	Pre-trip	Before the core power decay Core power decay at 24.4 s in the test	512	10.66
0~440 s	Post-trip	Before the SIT injection SIP injection at 52 s in the test SIT injection at 445 s in the test 1st loop seal clearing at 196 s in the test	1024	2.23
0~1000 s	Refill and long term cooling	All the interesting phenomena are included in this time frame	2048	1.02

Table 15. Summary of the Results of FFTBM to DSP-02 Calculation

Group	Phase relevant to PIRT	Time of interval					
		0 ~ 24 s		0~ 440 s		0 ~ 1000 s	
		N=512		N=1024		N=2048	
		AA_{tot}	WF_{tot}	AA_{tot}	WF_{tot}	AA_{tot}	WF_{tot}
A	A1 MARS-KS	0.173	0.126	0.228	0.094	0.280	0.090
	A2 MARS-KS	0.147	0.102	0.199	0.091	0.268	0.094
	A3 RELAP5/MOD3.3	0.151	0.129	0.238	0.090	0.290	0.094
B	B1 MARS-KS	0.398	0.086	0.467	0.070	0.523	0.076
	B2 RELAP5/MOD3.3	0.167	0.134	0.241	0.084	0.303	0.097
	B3 RELAP5-ME	0.145	0.123	0.252	0.105	0.298	0.076
	B4 MARS-KS	0.137	0.140	0.230	0.085	0.313	0.090
C	C1 MARS-KS	0.127	0.164	0.188	0.080	0.226[1)]	0.101
	C2 MARS-KS	0.164	0.132	0.247	0.098	0.324	0.084
	C3 MARS-KS	0.185	0.144	0.264	0.103	0.337	0.074
	C4 MARS-KS	0.170	0.134	0.243	0.098	0.320	0.083

1) Maximum calculation time is 595 s

the best prediction results among all participants. By comparing with the quantifications in the previous sections, the current FFTBM application results showed quite good consistency with them.

5.4. Accuracy Evaluation Results

The results of the accuracy evaluation for the time interval of 0-400 s are summarized in Table 16. Here, AA_{norm} in the table means the normalization to the results of the AA_{tot} calculation using the criteria of good prediction, e.g., 0.5, as mentioned in the previous section. The time interval for AA_{tot} or AA_{norm} was selected as 0-440 s as defined in Table 14, because most of the major phenomena, e.g., reactor trip, SIP injection, and loop seal clearing, occurred within the interval. The results of the accuracy evaluation are shown in Fig. 26.

As mentioned in the previous sections, the global acceptability factors, e.g. Q_A and Q_B, are identified as acceptable if they are less than 1.0. The normalized global accuracy, e.g., AA_{norm}, means a good prediction if it is less than 1.0, too. Thus, a combination of 3 global quantities can be meaningful for a quantitative comparison with the introduction of reasonable weighting relations between them. It is noteworthy here that an overall quantity called Q_{all} is introduced by the authors for a quantitative comparison between participants, as

$$Q_{all} = f_A \cdot Q_A + f_B \cdot Q_B + f_{AA} \cdot AA_{norm} \quad (6)$$

Table 16. Summary of Global Acceptability Factors and Average Accuracy Values

Participant	Q_A	Q_B	AA_{tot} [1)]	AA_{norm} [1)]	Q_{all} [2)]
A1	1.244	1.712	0.228	0.897	0.956
A2	0.716	0.159	0.199	0.783	0.699
A3	0.981	1.050	0.238	0.936	0.913
B1	NA	NA	0.467	1.837	1.669[3)]
B2	0.664	1.484	0.241	0.948	0.930
B3	1.727	1.318	0.252	0.991	1.041
B4	0.585	0.319	0.230	0.905	0.798
C1	0.716	1.449	0.188	0.739	0.765
C2	1.160	3.058	0.247	0.971	1.114
C3	2.009	1.046	0.264	1.038	1.081
C4	2.140	1.153	0.243	0.956	1.034

Note 1) The time interval is 0~440 s.
2) For the overall quantity, weighting factors of 0.2, 0.2, and 0.6 are considered for Q_A, Q_B, and AA_{norm}, respectively.
3) There are no data for Q_A and Q_B for participant B1, and the average Q_A and Q_B of all the other participants are assumed for the Q_{all} evaluation.

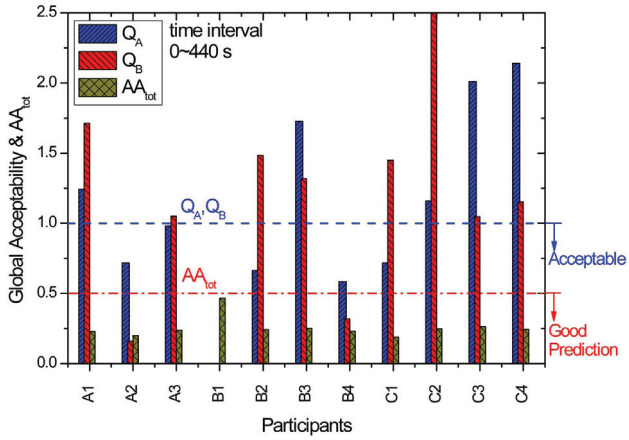

Fig. 26. Distribution of Global Acceptability Factors and Global Average Accuracy

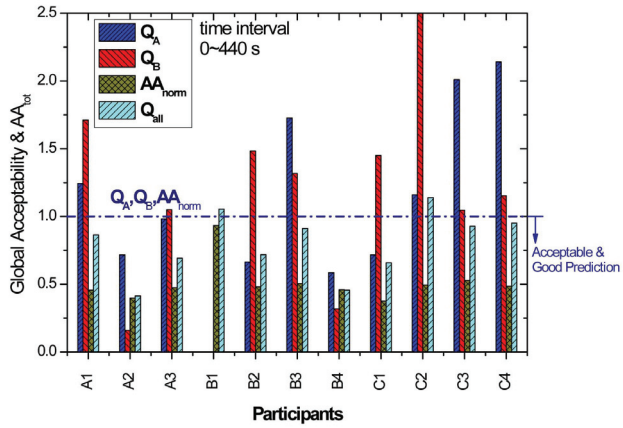

Fig. 27. Distribution of Global Acceptability Factors and Normalized Global Average Accuracy

The weighting factors f_A, f_B, and f_{AA} assumed in Table 16 were 0.2, 0.2, and 0.6, respectively. The results of the normalization are shown in Fig. 27.

6. CONCLUSIONS

The second domestic standard problem (DSP-02) was successfully completed using a 6-inch cold leg break loss of coolant accident data, where a total of 11 organizations including the research institute, industry, safety authority, and university contributed to in-depth safety analyses. Almost all participants used the MARS-KS code. Besides performing a comparison with the experimental data, each participant performed a sensitivity analysis on at least one special code assessment topic as agreed upon the organizing committee. This activity is expected to help find out the code deficiencies and obtain user guidelines that can minimize the "user effects."

In the DSP-02 exercise, the overall figure of merit for

a code accuracy quantification was fully applied. Three code accuracy quantification indices including (1) nodalization accuracy, (2) steady state accuracy, and (3) transient accuracy were defined and integrated to produce a single quantification index. The obtained outcomes will be used to improve the MARS-KS code model and help code users perform a safety analysis.

ACKNOWLEDGEMENTS

The authors are grateful to the Ministry of Education, Science and Technology (MEST) of Korea for their financial support for this project and to Korea Institute of Nuclear Safety (KINS) for their coordination support and analysis work.

NOMENCLATURE

A1~A3	Participants categorized into Group A
AFWP	Auxiliary feedwater pump
APR1400	Advanced power reactor 1400 MWe
ATLAS	Advanced Thermal-hydraulic test Loop for Accident Simulation
B1~B4	Participants categorized into Group B
BEMUSE	Best Estimate Methods Uncertainty and Sensitivity Evaluation
BS	Break simulator
C1~C4	Participants categorized into Group C
CL	Cold leg
CO	Core
CPU	Central process unit
CS	Containment simulator
DC	Downcomer
DP	Pressure difference
DCUH	Downcomer upper head
DSP	Domestic standard problem
DVI	Direct vessel injection
ECC	Emergency core cooling
EN2T	Environment & Energy Technology Co., Ltd.
FCV	Flow control valve
FDR	Facility Description Report
FFTBM	Fast Fourier transform based method
FLB	Feed line break
FNC	Future and Challenge Technology Co., Ltd.
HL	Hot leg
HPS	High pressure safety injection
ID	Identification or inner diameter
IET	Integral Effect Test
IL	Intermediate leg or cross-over leg (COL)
KAERI	Korea Atomic Energy Research Institute
KAIST	Korea Advanced Institute of Science and Technology
KEPCO	Korea Electric Power Corporation
KEPR	Korea Electric Power Research Institute
KINS	Korea Institute of Nuclear Safety
KEPCO NF	KEPCO Nuclear Fuel, Ltd.
KEPCO E&C	KEPCO Engineering and Construction Company, Inc.
LBLOCA	Large break loss of coolant accident
LC	Load cell
LOCA	Loss of coolant accident
LP	Lower plenum
LPP	Low pressurizer pressure trip
LSC	Loop seal clearing
LT	Level transmitter
LUDP	Low upper downcomer pressure trip
MARS-KS	Multi-dimensional analysis of reactor safety (version KS)
MF	Main feedwater
MS	Main steam
MSIV	Main steam isolation valve
MSLB	Main steam line break
MSSV	Main steam safety valve
NETEC	Nuclear Engineering & Technology Institute
OA	Operating agency, KAERI
OPR1000	Optimized power reactor 1000 MWe
OV	On-off valve
PCT	Peak cladding temperature
PT	Pressure transmitter
PWR	Pressurized water reactor
PZR	Pressurizer
QV	Volume flowmeter
RCP	Reactor coolant pump
RCS	Reactor coolant system
RELAP5	Reactor excursion and leak analysis program (version 5)
RETECH	Responsible Engineering Technology Co., Ltd.
RPV	Reactor pressure vessel
RV	Reactor vessel
RWT	Refueling water storage tank
SBLOCA	Small break loss of coolant accident
SD	Steam dome or system design
SDD	System Design & Development Co., Ltd.
SENTECH	System Engineering Technology Co., Ltd.
SG	Steam generator
SGSD	Steam generator steam dome
SGSDDC	Steam generator (between) steam dome (and) downcomer
SGTR	Steam generator tube rupture
SIP	Safety injection pump
SIT	Safety injection tank
SNU	Seoul National University
TC	Thermocouple
TF	Fluid temperature

Symbols

AA	Average amplitude (FFTBM) for a single parameter
AA_{norm}	Normalized AA_{tot} by 0.5
AA_{tot}	Global average amplitude (FFTBM) for the global calculation
AE	Architecture engineer or Acceptable error
Cd	Discharge coefficient
d	Diameter

E	Percentage error
f	Frequency or weighting factor
l	Axial length
Q	Heat loss
Q_A	Global acceptability factor for nodalization
Q_B	Global acceptable factor for steady state level
Q_i	Single acceptable factor
T	Temperature
DT	Temperature difference
WF	Weighted frequency
W_i	Weighting factor
Y_E	Experimental value of generic quantity

Subscripts

0R	model-to-prototype quantity ratio
1	primary system
2	secondary system
A	Q_A-related
AA	AA_{norm}-related
atm	atmospheric condition
B	Q_B-related
max	maximum
norm	normalized
s	sample
tot	total
w	wall

REFERENCES

[1] K.Y. Choi et al., "Comparison Report of Open Calculations for ATLAS Domestic Standard Problem (DSP-01), " KAERI /TR-4073/2010, Korea Atomic Energay Research Institute (2010).

[2] Y.S. Kim et al., "First ATLAS Domestic Standard Problem (DSP-01) for the Code Assessment," *Nuclear Engineering and Technology*, **43**, No.1, 25-44, (2011).

[3] K.Y. Choi et al., "ATLAS Domestic Standard Problem (DSP-02) Specifications," KAERI Internal Report, 53211-TS-002-R.03 (2011).

[4] K.H. Kang et al., "Detailed Description Report of ATLAS Facility and Instrumentation," KAERI/TR-4316/2011, Korea Atomic Energay Research Institute (2011).

[5] K.Y. Choi et al., "Comparison Report of Open Calculations for ATLAS Domestic Standard Problem (DSP-02), " KAERI /TR-4574/2012, Korea Atomic Energay Research Institute (2012).

[6] Y.S. Kim, K.Y. Choi, H.S. Park, S. Cho, B.D. Kim, N.H. Choi, W.P. Baek, "Commissioning of the ATLAS thermal-hydraulic integral test facility," *Annals of Nuclear Energy*, **35**, 1791-1799 (2008).

[7] K.Y. Choi, H.S. Park, S. Cho, D.J. Euh, Y.S. Kim, W.P.Baek, "Integral Behavior of the ATLAS Facility for a 3-inch Small Break Loss of Coolant Accident," *Nuclear Engineering and Technology*, **40**, 199-212, (2008).

[8] M. Ishii and I. Kataoka, "Similarity Analysis and Scaling Criteria for LWRs Under Single Phase and Two-Phase Natural Circulation," NUREG/CR-3267, ANL-83-32, Argonne National Laboratory (1983).

[9] H. S. Park et al., "An Assessment of a LBLOCA Similarity for a Reduced-Height Integral Effect Test Loop Design for PWRs," *Annals of Nuclear Energy*, **34**, 931-937 (2007).

[10] S. Cho, et al., Quick loop report on the 6 inch cold leg SBLOCA test with the ATLAS, Technical Report for the SPACE code, S06NX08-A-1-TR-09, (2011).

[11] A. Petruzzi and F.D'Auria, "Re-analysis of the ISP-13 Exercise, Post Test Analysis of the LOFT L2-5 Test Calculation," BEMUSE Phase II Report, NEA/CSNI/R (2006)2, (2006).

[12] A. Prosek, F. D'Auria, B. Mavko, "Review of Quantitative Accuracy Assessments with Fast Fourier Transform Based Method (FFTBM)," *Nuclear Engineering and Design*, 217, 179-206, (2002).